Journal of Modeling and Simulation of Microsystems, Vol. 2, No. 1, Pages 21-34, 2001.

MODELING OPTICAL MEM SYSTEMS

T.P. Kurzweg†, J.A. Martinez, S.P. Levitan, and M.T. Shomsky
Department of Electrical Engineering, University of Pittsburgh, Pittsburgh, PA 15261, U.S.A.

P.J. Marchand
Department of Electrical and Computer Engineering, University of California/San Diego, La Jolla, CA 92093, U.S.A.

D.M. Chiarulli
Department of Computer Science, University of Pittsburgh, Pittsburgh, PA 15261, U.S.A.

Abstract

Optical MEMS have the potential to drastically reduce the size and cost of digital communications and computation systems. However, the multiple technologies (optical, electrical, and mechanical) utilized in optical MEM systems has led to new challenges in the creation of computer aided design tools for these systems. This paper presents a system level opto-electro-mechanical CAD tool, Chatoyant, developed to meet the needs of mixed technology systems designers. We introduce signal models and analysis techniques that enable our tool to support optical MEMS design. We demonstrate these results with the analysis of two mixed-signal systems: a full opto-electronic communications link and an actively aligned optical MEM beam steering system.

Keywords: Optical modeling, MEMS, MOEMS, systems

1. Introduction

For integrated micro-systems composed of electrical, optical, and mechanical components, the need to model large numbers of linear and non-linear components with sufficient accuracy to analyze cross-talk, noise, and tolerancing in a interactive environment leads to the requirement of an efficient yet accurate mixed-technology simulation technique. Beyond functional design, mixed technology tools, working at the system level, must support the traditional models of performance (e.g., speed, power, and area) as well as the special needs of mixed technology systems, such as noise, crosstalk, and mechanical tolerancing. Most importantly, the tools must be able to capture the interaction of these constraints in order to support the designer in making both architectural and technological tradeoffs. These requirements imply a need for high level models for optical, optoelectronic, and electromechanical micro-components, accurate and computationally efficient simulation, and an expanded scope for performance and reliability modeling. Currently, no single CAD tool completely models the complexity of these mixed-signal systems. Therefore, designers must use a collection of tools to model, simulate, and analyze each stage of the design. We attempt to fill this void with our tool.

Our work began with the investigation of methods for modeling digital free space optoelectronic systems. These are systems that incorporate electronic digital and analog components, optoelectronic interface devices, such as laser and detector arrays, and free space optical interconnects including passive and active optical elements. These models have been successfully incorporated into an optoelectronic system-level design tool called Chatoyant [1,2]. However, these tools and algorithms were predicated on the use of macro-scale optoelectronic components with system dimensions on the order of meters down to millimeters. While such systems have been built, and are continuing to show utility in such applications as high-speed communications, new device and fabrication technology is enabling micro-scale optoelectronic systems. The confluence of system on a chip (SOC) integration levels with new micro-scale optical, optoelectronic, and electromechanical components has enabled the fabrication of an entirely new class of systems, optical micro-electro-mechanical systems (OMEMS).

Recently, we have extended Chatoyant to support modeling and simulating of micro-opto-electro-mechanical systems by including micro-optical and mechanical components, along with a tolerancing analysis package for the precise alignment required for the correct operation of these systems [3,4]. This has enabled us to simulate and analyze mixed-signal optical MEM systems, by modeling both the individual signals and their interactions, while performing system level analyses. In this paper, we present the features of Chatoyant that are useful in the modeling, simulating, and analysis of optical MEM systems. We first present an overview of system level modeling for mixed-technology systems. Next, we introduce electrical, mechanical, and optical models that are used as building blocks in optical MEM system design. We then focus on two optical mixed-signal systems simulated within Chatoyant and present results that illustrate our model implementations and analysis techniques.

†. tim@ee.pitt.edu

2. Mixed-Signal Optical MEM Simulation Tool: Chatoyant

Chatoyant, is a multi-level, multi-domain CAD tool that has been successfully used to design and simulate free space optoelectronic interconnect systems [1,5]. Static simulations analyze mechanical tolerancing, power loss, insertion loss, and crosstalk, while dynamic simulations are used to analyze data streams with techniques such as noise analysis and bit error rate (BER) calculation. Chatoyant is based on a methodology of system level architecture design. In this methodology, architectures are defined in terms of models for "modules", the "signals" that pass between them, and the "dynamics" of the system behavior. For electrical, mechanical, and optical systems, our signals are represented as electronic waveforms, mechanical deformations, and modulated carriers, i.e., beams of light. Using the characteristics of these signals, we define models for the system components in terms of the ways they transform the characteristic parameters of these signals.

Chatoyant is built upon the object-oriented simulation engine Ptolemy [6]. Chatoyant's component models are written in C++ with sets of user defined parameters for the characteristics of each module instance. The signal information is carried between modules using a "message class". To maximize our modeling flexibility, our signals are composite types, representing the attributes of position and orientation for both optical and mechanical signals, voltages and impedances for electronic signals, and wavefront, phase, and intensity for optical signals. The composite type is extensible, allowing us to add new signal characteristics as needed. The Ptolemy simulation method used in Chatoyant is called "Dynamic Data Flow" (DDF) with the modification that timing information is added to each message to support multiple and run-time-rate variable streams of data flowing through the system, which is essential for multiple domains.

Component models are based on three modeling techniques. The first is a "derived model" technique. That is, analytic models based on an underlying physical model of the device. These can be very abstract "0th-order" models, or more complex models involving time varying functions, internal state, or memory. The second class of models is based on empirical measurements from fabricated devices. These models use measured data and interpolation techniques to directly map input signal values to output values. The third technique is reduced order or response surface models. For these models, we use the results of low level simulations, such as finite element solvers, or simulators, and generate a reduced order model, which covers the range of operating points for the component by producing a polynomial curve fit, or simple interpolation over the range of operation. We have successfully used all three of these methods in the creation of four component libraries. The Optoelectronic Library includes vertical cavity surface emitting lasers (VCSELs), multiple quantum well (MQW) modulators, and p-i-n detectors. The Optical Library contains components such as refractive and diffractive lenses, lenslets, mirrors, and apertures. The Electrical Library includes CMOS drivers and transimpedance amplifiers, and the Mechanical Library contains scratch drive actuators and other electro-static devices.

In the remainder of this section, we present our techniques for system level modeling, followed by the methodologies for electrical, mechanical, and optical signal modeling.

2.1. System Simulation

As previously mentioned, the simulation of optical MEM systems involves signals of very different structures with varied dynamics. The use of the object-oriented Ptolemy framework permits a large degree of abstraction for the simulation of such systems. This is in contrast to simulators based on potential/field gradients or finite element analysis. In Ptolemy's abstraction framework, the system is decomposed into component modules that are individually characterized and joined together by the mutual exchange of information. The nature of this information can be optical, electrical, mechanical, or any combination of these.

The information flow is handled using a "message class", a heterogeneous interface that allows for the transmission of a token, or particle, of data information between components. The advantage of using such a class is that one single message contains optical, electrical, or mechanical information, and each component type-checks the data, extracting the relevant information. The message class also carries time information for each message in the stream of data. This allows for the dynamic insertion and deletion of samples by any component, as discussed below.

In this model of computation, the simulation scheduler creates a dynamic schedule based on the flow of data between the modules. In other words, the order of the modules' execution is set during run time. This allows modeling of multi-dynamic systems where every component can alter the rate of consumed/produced data during simulation. The scheduler also provides the system with buffering capability. This allows the system to keep track of all the particles arriving at one module when multiple input streams of data are involved.

Before the discussion of individual signal models and to further understand the development of our system-level simulation tool, we first introduce our device and component modeling methodology.

2.1.1. Device and component models

We make a distinction between device level and component level modeling. Device level models focus on explicitly modeling the processes within the physical geometry of a device such as fields, fluxes, stresses, and thermal gradients. Conversely, in component level models these distributed effects are characterized in terms of device parameters, and the models focus on the relationships between these parameters and state variables (e.g., optical intensity, phase, current, voltage, displacement, or temperature) as a set of linear or non-linear differential equations (DE). In the electronic domain these are called "circuit models."

Circuit-level (or more generally, component-level) modeling techniques can be used for optoelectronic device modeling, but, for most models, the degree of accuracy does not match that required for performance analysis in these type of devices. Fast Transient phenomena, dependencies on the physical geometry of the device, and large signal operation

are generally not well characterized by these kinds of models. On the other hand, device level simulation techniques offer the degree of accuracy required to model fast transients (e.g., chirp), fabrication geometry dependencies, as well as steady-state solutions in the optical device [7]. However, modeling these processes requires specialized techniques and large computational resources. Further, these simulations produce results that are generally not compatible with the specialized simulators required for other domains. For instance, it is difficult to model the behavior of a laser in terms of carrier population densities, and at the same time, the emitted light in terms of its electro-magnetic fields.

There are two basic techniques to deal with this problem of device simulation vs. circuit simulation. The first is the use of two levels of simulation, a device level simulation for each unique domain, coupled to a common circuit level simulation that coordinates the results of each. The idea is analogous to the technique of using a digital simulation backbone to tie together analog simulations for mixed-signal VLSI. However, for the case of device and circuit co-simulation, this technique has all the drawbacks previously mentioned for the device level simulation and the additional computational resources to coordinate both simulators and make them converge to a common point of operation [8,9].

Rather, our approach is to increase the accuracy of the circuit-level (component level) models. That is, to incorporate the transient solution, along with other second order effects, of the device analysis within the circuit level simulation. This is accomplished by creating circuit models for these higher order effects and incorporating them into the circuit model of the optoelectronic device. Different methodologies could be used to translate the device level expressions, which characterize the semiconductor device operation (e.g., Poisson's, the carrier current, and the carrier continuity equation) into a set of temporal linear/non-linear differential equations [7,10]. The advantage of having this representation is that we can simulate electronic and optoelectronic models in a single mixed-domain component level simulator.

Our component models fit well with the Ptolemy simulation engine. It allows a conceptual and abstract representation of the system consisting of a set of modules interchanging information (energy signals). However, this approach brings the challenge of choosing which circuit/component modeling techniques will be optimal for accurate and fast characterization of the different modules involved in this system.

2.1.2. Simulation issues

Traditional circuit simulators based on numerical integration solvers offer the required accuracy to solve linear and non-linear DE systems, however, they are too computationally expensive to consider for evaluating individual modules in a mixed domain framework [11,12]. In the linear case, successful low order reduction techniques have been used to model high-density interconnection networks with excellent computational efficiency [13-16]. In the non-linear case, however, the success is only partial. Work has been conduced to apply reduction techniques to obtain macro-models for the interconnection section and use them in circuit simulators, such as SPICE [17], as a way to simplify the computational task carried on by such solvers [12,16]. Merging both techniques maintains the accuracy offered by circuit simulators, but also the problems associated with them.

Two problems with this technique are the difficulties guaranteeing the convergence of the solution and the relatively high computational load. Pioneer non-linear network modeling using piece-wise models in a timing simulator RSIM [18] was conducted by Kao and Horowitz [19]. While well suited for delay estimation in dense non-linear networks, the limited complexity of models and tree analysis technique used do not allow piecewise linear timing analyzers to simulate higher order effects which are of significant importance in the modeling of typical optoelectronic devices.

The fact that the density of the network generated for modeling of our opto-electro-mechanical devices is moderate allows us to consider piecewise linear (PWL) modeling merged with linear numerical analysis as a way to achieve the desired accuracy with a lower computational demand. More importantly, the amount of feedback between active devices in such models is limited, when compared with dense VLSI networks, which makes the scheduling task feasible even for increased numbers of regions of operation for each device.

For simulation, we perform a linear numerical analysis in order to solve the DE set necessary to obtain an accurate solution, using piecewise modeling to overcome the iteration process encountered in the integration technique used in traditional circuit simulators for the non-linear case. Linearizing the behavior of the non-linear devices by regions of operation simplifies the computational task to solve the system. This also allows us to trade accuracy for speed. Most importantly, PWL models for these devices allow us to integrate mechanical, electrical and optical components in the same simulation. We have successfully used this technique to model electric and optoelectronic components and are currently expanding this same methodology to incorporate mechanical models. These models will be discussed next.

2.2. Optoelectronic Models

2.2.1. Piecewise linear electrical modeling

Our optoelectronic modeling is accomplished as shown in Fig. 1. We perform linear and non-linear sub-block decomposition of the circuit model of the device. This decomposes the design into a linear multi-port sub-block section and non-linear sub-blocks. The linear multi-port sub-block can be thought of as characterizing the interconnection network or parasitics while the non-linear sub-blocks characterize the active devices.

Then, Modified Nodal Analysis (MNA) [20] is used to create a matrix representation for the device, shown in Fig. 2. In this expression, $[S]$ is the storage element matrix, $[G]$ is the conductance matrix, $[x]$ is the vector of state variables, $[b]$ is a connectivity matrix, $[u]$ is the excitation vector, and $[I]$ is the current vector.

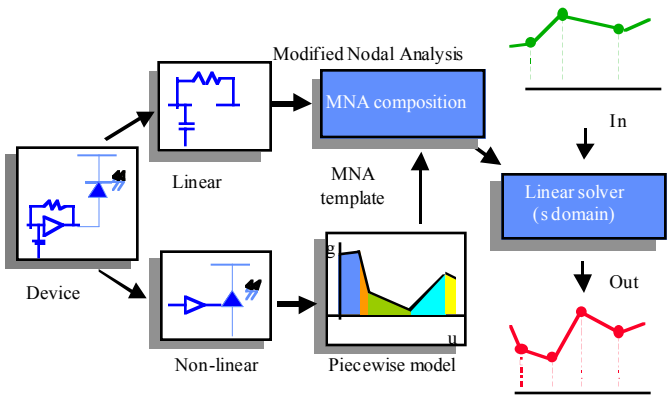

Fig. 1: Piecewise Modeling for Electical/Optoelectical Devices.

The linear sub-block elements can be directly matched to this representation but the non-linear elements need to first undergo a further transformation. We perform piecewise modeling of the active devices for each non-linear sub-block. When we form each non-linear sub-block, a MNA template is used for each device in the network. The use of piecewise models is based on the ability to change these models for the active devices depending on the changes in conditions in the circuit, and thus the regions of operation.

The templates generated can be integrated to the general MNA containing the linear components adding their matrix contents to their corresponding counterparts. This process is shown in Fig. 2 for the *S* matrix. This same composition is done for the other matrices. The size of each of the template matrices is bounded to the number of nodes connected to the non-linear element.

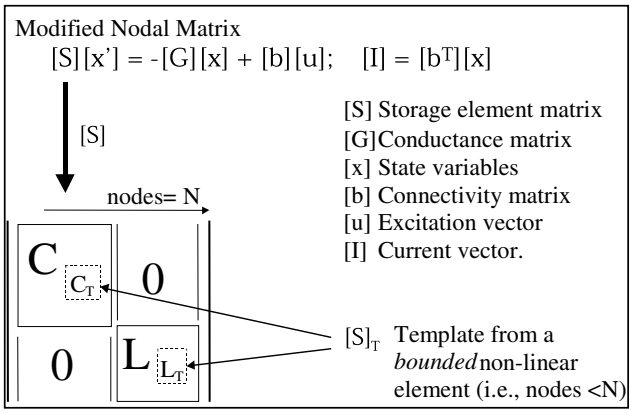

Fig. 2: MNA Representation and Template Integration.

Once the integrated MNA is formed, a linear analysis in the frequency domain can be performed to obtain the solution of the system. Constraining the signals in the system to be piecewise in nature allows us to use simple transformation to the time domain without the use of costly numerical integration.

During each time step in the simulation, the state variables in the module will change and might cause the active devices to change their modes of operation. Therefore, we re-compute and re-characterize the PWL solution caused by changes between piecewise models. Depending on the number of segments used in the piecewise linear model, on average there will be a large number of time steps during which the system representation is unchanged, justifying the computational savings of this technique.

Understanding that the degree of accuracy of piecewise linear models depends mainly on the step size chosen for the time base, an adaptive control method for the time steps is added to the models [20]. A binary search over the time step interval is the basis for this dynamic algorithm. The algorithm discards non-significant samples, which do not appreciatively affect the output, and adds samples when the output change is greater than a user defined tolerance. The inclusion of the samples during fast transitions or suppression of time-points during "steady state" periods optimizes the number of events used in the simulation.

To support electrical signals, Chatoyant's message class contains parameters that represent general electrical signals that are passed between electrical devices. Three parameters that are in the message class for electrical signals are output potential, V, capacitance, C_{sb}, and conductance, g_{sb}. The last two fields define the output impedance of the signal, aiding impedance matching between electrical devices. We next show an example of how we use our electrical technique in the modeling of CMOS circuits.

2.2.2. Modeling of CMOS circuits

To illustrate our modeling of the active optoelectronic devices in modular networks, we focus on CMOS driver circuits based on the simple complementary inverter. Considering the classical non-linear V-I equations for MOS transistors (Level II) as characterizing the behavior of every FET device, a linearization of drain-source current (I_{ds}) is presented using:

$$\Delta I_{ds} = g_m(P)\Delta v_{gs} + g_{ds}(P)\Delta v_{ds}, \qquad (1)$$

where, P represents the piecewise linear region of operation for the device. Transconductance (g_m) and conductance (g_{ds}) are the parameters characterizing the device. In Fig. 3 (a), the parasitic effects (C_{ds}, C_{gs}, and C_{ds}) are introduced. A MNA template is created from this representation and is shown in Fig. 3 (b). This MNA formulation allows us to incorporate the FET as a three-port element into the MNA of a complete optoelectronic module. The non-linear nature of the FET is modeled by piecewise changes in values of the parameters (g_{ds}, g_m, C_{ds}, C_{gs}, and C_{ds}) depending on the region of operation and are thus functions of V_g, V_d, and V_s.

To show the speed and accuracy of the PWL approach, we performed several experiments comparing our results to that of Spice 3f4 (Level II). The test was a multistage amplifier with a significant number of drivers. PWL models were tested versus Spice at 10 and 1000 *MHz*. Fig. 4 shows that the speed up achieved for the same number of timepoints is at least two orders of magnitude faster than Spice. Accuracy was less than 10% RMS error. These results show that PWL models are well suited to perform accurate and fast simulations for the typical multistage CMOS drivers and transimpedance amplifiers widely used in optoelectronic applications. In the next section, we show how this same procedure for modeling electronic signals can be extended for modeling mechanical structures.

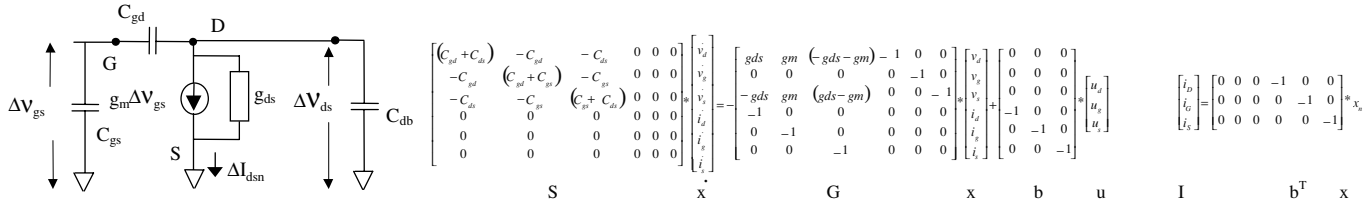

(a) (b)

Fig. 3: MFET (a) Model (b) Template.

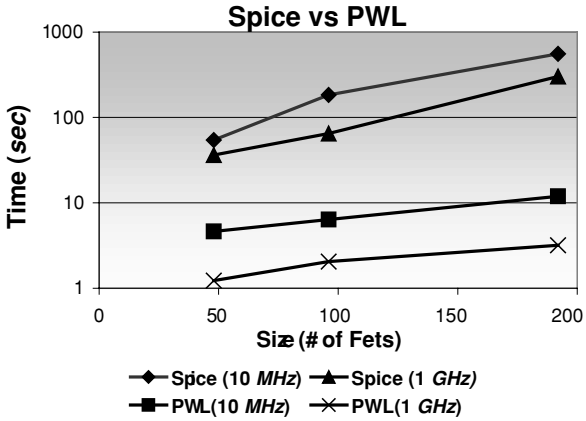

Fig. 4: Spice vs. PWL Models in a System of Multiple FETs.

2.3. Mechanical Models

The general module for solving sets of non-linear differential equations using PWL can be used to integrate complex mechanical models in our design tool. The model for a mechanical device can be summarized in a set of differential equations that define its dynamics as reaction to external forces. This model then must be converted to the form seen in the electrical case to be given to the PWL solver for evaluation.

In the field of MEM modeling, there has been an increasing amount of work that uses a set of Ordinary Differential Equations (ODEs) to characterize MEM devices [21-23]. ODE modeling is used instead of techniques such as finite element analysis, to reduce the time and amount of computational resources necessary for simulation. The model uses non-linear differential equations in multiple degrees of freedom and in mixed domains. The technique models a MEM device by characterizing its different basic components such as beams, plate-masses, joints, and electrostatic gaps, and by using local interactions between components.

Our approach to modeling mechanical elements is to reduce the mechanical ODE representation to a form matching the electronic counterpart, seen in the equation in Fig. 2. This enables the use of the piecewise linear technique previously discussed for simulating the dynamic behavior of electrical systems.

With damping forces proportional to the velocity, the motion equation of a mechanical structure with viscous damping effects is [22]:

$$F = [K]U + [B]V + [M]A\,, \tag{2}$$

where, $[K]$ is the stiffness matrix, U is the displacement vector, $[B]$ is the damping matrix, V is the velocity vector, $[M]$ is the mass matrix, A is the acceleration vector, and F is the vector of external forces affecting the structure. Obviously, knowing that the velocity is the first derivative and the acceleration is the second derivative of the displacement, the above equation can be recast to:

$$F = [K]U + [B]U' + [M]U'' \tag{3}$$

Similar to the electrical modeling, this equation represents a set of linear ODEs if the characteristic matrices $[K]$, $[B]$, and $[M]$ are static and independent of the dynamics in the body. If the matrixes are not static and independent (e.g., aerodynamic load effect), they represent a set of non-linear ODEs.

To reduce the above equation to a standard form, we use a modification of Duncan's reduction technique for vibration analysis in damped structural systems [24]. This modification allows for the above general mechanical motion equation to be reduced to a standard first order form, similar to Equation 1, which allows complete characterization of a mechanical system.

$$\begin{bmatrix} 0 & M \\ M & B \end{bmatrix}\begin{bmatrix} U'' \\ U' \end{bmatrix} + \begin{bmatrix} -M & 0 \\ 0 & K \end{bmatrix}\begin{bmatrix} U' \\ U \end{bmatrix} = \begin{bmatrix} 0 \\ I \end{bmatrix} F \tag{4}$$

Using substitutions, the equation is rewritten as:

$$[Mb]X' + [Mk]X = [E]F\,, \tag{5}$$

where the new state variable vector $X = \begin{bmatrix} U' \\ U \end{bmatrix}$.

Each mechanical element (beam, plate, etc.) is characterized by a template consisting of the set of matrices $[Mb]$ and $[Mk]$, composed of matrices $[B]$, $[M]$, and $[K]$ in the specified form seen above. If the dimensional displacements are constrained to be small and the shear deformations are ignored, the derivation of $[Mb]$ and $[Mk]$ is simplified and independent of the state variables in the system. Additionally, the model for elements is formulated assuming a one-element idealization (e.g., two nodes for a beam). Consequently, only the static resonant mode is considered. Multiple-element idealization can be performed combining basic elements to characterize higher order modes.

As an example of our mechanical technique, we present the

response of an anchored beam in a 2D plane with an external force applied on the free end. The template for the constrained beam is composed of the following matrices [25]:

$$M = \frac{EI_z}{l^3}\begin{bmatrix} \frac{Al^2}{I_z} & 0 & 0 \\ 0 & 12 & -6l \\ 0 & -6l & 4l^2 \end{bmatrix}; M = \frac{\rho Al}{420}\begin{bmatrix} 140 & 0 & 0 \\ 0 & 156 & -22l \\ 0 & -22l & 4l^2 \end{bmatrix}; \quad (6)$$

$$B = \delta\begin{bmatrix} 1 & 0 & 0 \\ 0 & 1 & 0 \\ 0 & 0 & 1 \end{bmatrix}$$

where, E is Young's modulus, I_z is the inertia momentum in z, A is the area of the beam, l is the length, δ is the density of the material, and ρ is the viscosity factor in the system acting over x and y components.

The analysis of this element is obtained using the piecewise linear technique presented above. Constraining the input/ output signals to a piecewise linear wave, the time domain response is completed in one step, without costly numerical integration.

To test our results, a comparison against NODAS [22] was performed. Fig. 5 shows the frequency response and corresponding resonant frequencies for this constrained beam (183 μm length, 3.8 μm width, poly-Si) from both our PWL technique and NODAS. The transient response to 1.8 nN non-ideal step (rise time of 10 μsec) rotational torque is also simulated. The rotational deformation to this force is shown in Fig. 6. The comparison between our results and NODAS's are very close. NODAS uses SABER, a circuit analyzer performing numerical integration for every analyzed point, which results in costly computation time. Our linear piecewise solver is computational intensive during the eigenvalue search, however, this procedure is performed only one time at the beginning of the simulation run. We believe that this will result in a more computationally efficient simulation. However, as previously mentioned, the accuracy of the analysis depends in the granularity of the piecewise characterization for the signals used in the system, which can increase computation time.

Typically, this beam is only a part of a bigger device made from individual components that are characterized using similar expressions. The generalization of the previous case to an assembly of elements or mechanical structure is fairly straightforward. The general expression, seen in Equation 3, characterizes the whole structure defined by a set of nodes, from which every individual element shares a subset. The next step, similar to the previously considered electronic case, is merging the individual templates together, composing the general matrix representation for the composed structure. However, a common coordinate reference must be used for this characterization of mechanical structures since every template or element is characterized in a local reference system. The process of translation of these local templates to the global reference system can be described by [25]:

$$S = A^T \bar{S} A \quad (7)$$

where, A represents the translation matrix from local displacements to global displacements (a function of the structure's geometery), $\bar{S}$ represents the local template, and S is the corresponding global representation. The next step is the addition of these global representations into the general matrix form, using the matrices' nodal indexes as reference. Finally, the piecewise linear solver can be used on the composed system's general matrix and simulated.

The use of a PWL general solver for mechanical simulation decreases the computational task and allows for a trade-off between accuracy and speed. The additional advantage of using the same technique to characterize electrical and mechanical models allows us to easily merge both technologies in complex devices that interact in mixed domains.

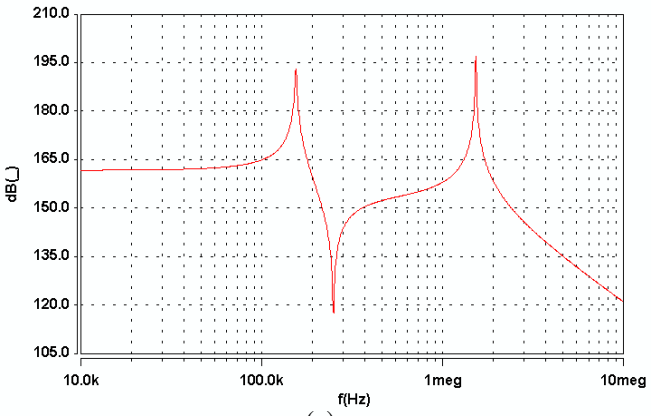

(a)

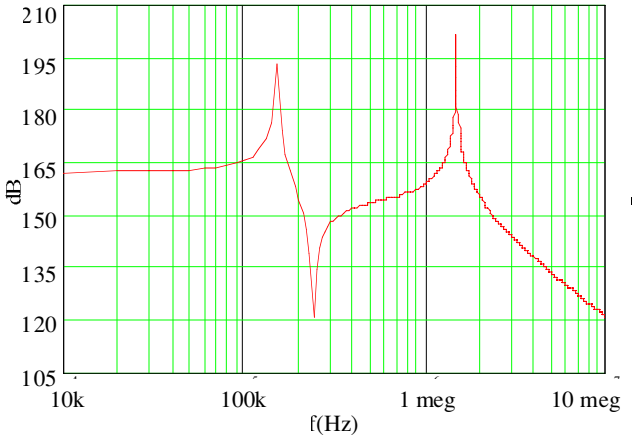

(b)

	Resonance Frequencies	
	f_1	f_2
Nodas	154.59kHz	1.52MHz
PWL simulator	150.04kHz	1.48MHz

Fig. 5: Frequency Response of a Beam: (a) NODAS (b) Chatoyant.

2.4. Optical Propagation Models

Our optical propagation models are based on two techniques: Gaussian and diffractive scalar. Gaussian models give us fast, accurate results for marco-scale systems and systems that

exhibit limited diffraction. Slower diffractive scalar models must be used when diffraction effects dominate the system.

2.4.1. Gaussian models

The optical propagation is based on Gaussian beam analysis, allowing paraxial light to be modeled by nine scalar parameters, and components to be modeled by an optical ABCD matrix, which describes how light is effected by a component [1]. The Gaussian beam is defined by the parameters seen in Table 1.

As the parameters in the table discretely allude to, our optical propagation is actually a mixture of ray analysis and Gaussian analysis. We first find the position and direction of the center of the Gaussian beam, using typical ray methods. We then "superimpose" the Gaussian beam over this ray-traced beam to model intensity, waist, phase, and depth of focus. The advantage of using Gaussian beam analysis is in the computational speed in which propagated light can be modeled. This allows for interactive system level design, however, for some micro systems, where diffractive effects dominate, another optical propagation method has to be used, as seen later.

These nine scalar parameters are contained in Chatoyant's message class, and passed between components. It is the component's responsibility to "construct" the beam from the parameters, alter the beam according to its function, and "decompose" the beam back into parameters, which are returned to the message class and passed to the next object. Using Gaussian beam propagation, components are modeled with the previously mentioned ABCD matrix. For example, we examine the interaction between a Gaussian beam and a thin lens. To study the beam/lens interaction, we start with a definition of the Gaussian beam's q-parameter, which characterizes a Gaussian beam of known peak amplitude [26]:

$$q = zw0 + jz0\,, \tag{8}$$

where, the real part is the distance to the minimum waist, and the imaginary is the Rayleigh range, from which the waist of the beam is determined. The new Gaussian beam is defined by the following:

$$q_2 = \frac{Aq_1 + B}{Cq_1 + D}\,, \tag{9}$$

where, *ABCD* is the matrix that defines a component. In the case of a thin lens, A=1, B=0, C=-1/f, D=1, where f is the focal length of the lens. Solving for q_2, and determining the real and imaginary parts, the new $z0'$ and $zw0'$ for the emerging Gaussian beam can be found:

$$z0' = \frac{f^2 \cdot z0}{(f - zw0)^2 + z0^2} \tag{10}$$

$$zw0' = \frac{f(f \cdot zw0 - zw0^2 - z0^2)}{(f - zw0)^2 + z0^2} \tag{11}$$

The position and direction of the beam is determined from common Ray tracing techniques:

$$y_2 = Ay_1 + B\theta_1 \qquad \theta_2 = Cy_1 + D\theta_1 \tag{12}$$

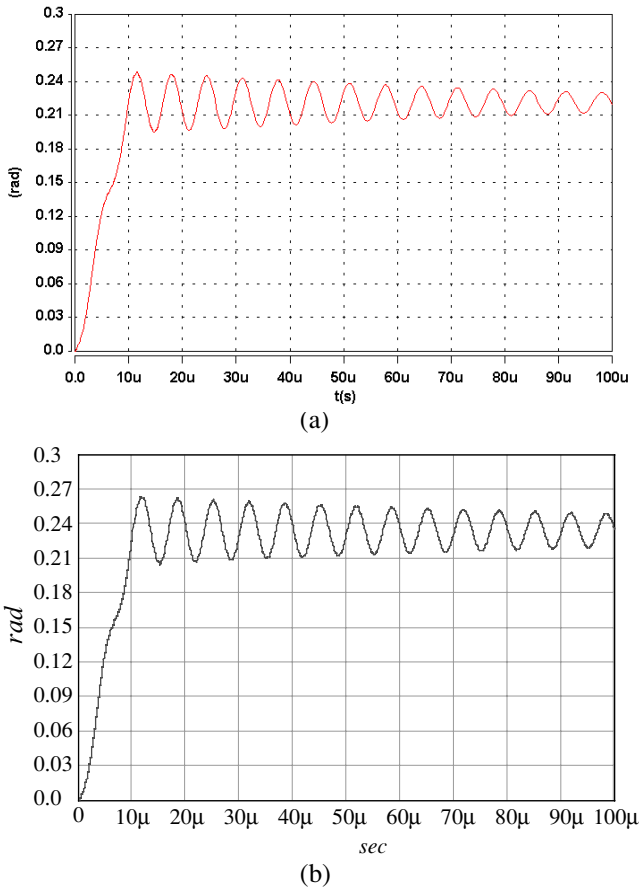

Fig. 6: Transient Response of a Beam: (a) NODAS (b) Chatoyant.

Table 1: Gaussian Beam Parameters.

Parameter	Description
x,y	Center position of the Gaussian beam
Rho, theta	Directional cosines of the Gaussian beam
Intensity	Peak intensity of the Gaussian beam
z0	Rayleigh range, or depth of focus
Zw0	Distance to the next minimum waist
Lambda	Wavelength of the light
Phase	Phase of the central peak of the beam

However, as the systems that we wish to design continue to diminish in size, diffractive effects are a major concern. For example, in optical MEM design, the size of the components, apertures, and small structures bring diffractive effects into play, along with the use of diffractive elements such as Fresnel zone plates, binary lenses, gratings, and computer generated holograms (CGH) [27]. Therefore, new design tools are needed that utilize optical models that can provide accurate diffractive results with reasonable computational costs. In addition to diffractive effects, other characteristics of optical signals are important, such as polarization, scattering, phase, frequency (wavelength) dependence, and dispersion. This last being a requirement for modeling fiber optic components.

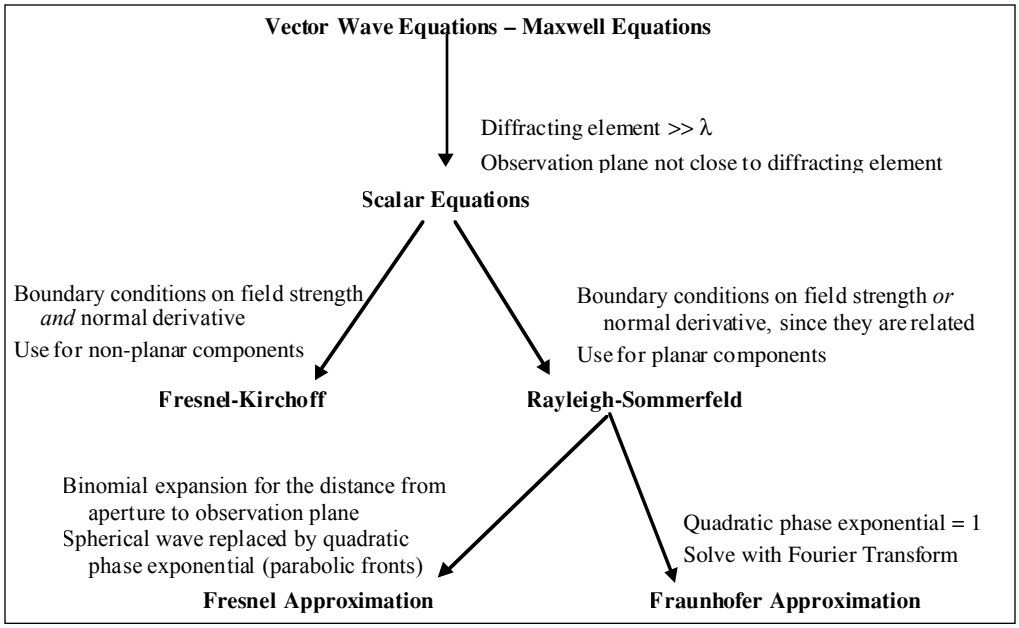

Fig. 7: Scalar Modeling Techniques.

2.4.2. Scalar diffractive models

A diffractive optical propagation methodology is required to model light propagating through small sized components and the diffractive elements found in optical MEM systems. To identify which modeling technique is best suited for our implementation, we need to analyze the optical MEM systems that we wish to model and evaluate the available optical propagation techniques. Current optical MEM systems have component sizes of roughly ten to hundreds of microns and propagation distances in the hundreds of microns. With these sizes and distances on the order of ten to a thousand times the wavelength of light, optical diffractive models are required. Fig. 7 is a tree that begins at the top with the vector wave equations, or Maxwell's equations, and branches through the different abstraction levels of scalar modeling techniques. Along the arrows, notes are added stating the limitations and approximations that are made for each formulation. We start our search for the appropriate optical propagation method with scalar diffraction models, due to our intuition that these models will be accurate in the optical MEM domain, and have a smaller computation time than the full vector method.

Scalar equations are directly descended from Maxwell's Equations. Maxwell equations, with the absence of free charge, are [28-30]:

$$\nabla \times \vec{E} = -\mu \frac{\partial \vec{H}}{\partial t} \qquad \nabla \times \vec{H} = -\varepsilon \frac{\partial \vec{E}}{\partial t}$$
$$\nabla \bullet \varepsilon \vec{E} = 0 \qquad \nabla \bullet \mu \vec{H} = 0 \tag{13}$$

These equations can be recast into the following form:

$$\nabla^2 \vec{E} - \frac{n^2}{c^2} \frac{\partial^2}{\partial t} \vec{E} = 0 \qquad \nabla^2 \vec{H} - \frac{n^2}{c^2} \frac{\partial^2}{\partial t} \vec{H} = 0 \tag{14}$$

If we assume that the dielectric medium is linear, isotropic, homogeneous, and nondispersive, all components in the electric and magnetic field can be summarized by the scalar wave equation:

$$\nabla^2 \vec{U} - \frac{n^2}{c^2} \frac{\partial^2}{\partial t} \vec{U} = 0 \tag{15}$$

For monochromatic light, $U(P,t)$ is the positional complex wave function, where P is the position of a point in space:

$$U(P,t) = a(P) e^{j\varphi(P)} e^{j2\pi v} \tag{16}$$

By placing the positional complex wave function into the scalar wave equation, the result is the time-independent Helmholtz equation, which every scalar wave must satisfy:

$$(\nabla^2 + k^2) U(P) = 0, \tag{17}$$

where, $k = \frac{2\pi}{\lambda}$

The challenge is to determine the scalar wave function as it propagates through a diffractive element. One answer is based on the Huygens-Fresnel principle that states that every unobstructed point of a wavefront at a given time serves as a source of spherical wavelets with the same frequency as the primary wave. The Huygens-Fresnel principle mathematically describes the Rayleigh-Sommerfeld scalar diffraction formulation:

$$U2(x,y) = \frac{z}{j\lambda} \iint U1(\xi,\eta) \frac{e^{jkr_{12}}}{r_{12}^2} \partial\xi \partial\eta, \tag{18}$$

where, ξ and η are the coordinates of the aperture plane, and x and y are the coordinates of the obsevation plane.

All scalar diffraction solutions are limited by two assumptions; the diffracting structures must be "large" compared with the wavelength of the light and the observation screen can not be "too close" to the diffracting

structure. However, these dimensions are not clearly defined, questioning if scalar optical models are valid for all optical MEM systems. For some extremely small optical MEM systems, our initial intuition of "adequate" scalar models, might be invalid, and full wave propagation models must be used.

When modeling scalar formulations, explicit integration of the wave front is performed at each interface, severely increasing the computation time. Using approximations to the scalar formulations, as seen in Fig. 7, can reduce this time. For example, the Fraunhofer approximation is solved using a Fourier transform, where common FFT algorithms enable an efficient solution. However, the valid propagation ranges limit when these approximations can be used. Fig. 8 shows where these different modeling techniques are valid with respect to the distance propagated past a diffracting element.

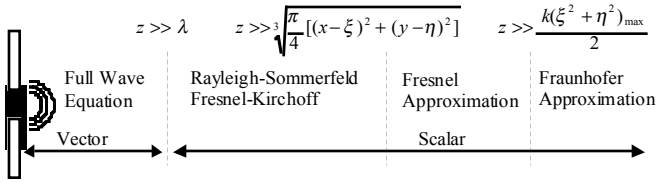

Fig. 8: Valid Propagation Distances of Scalar Modeling Techinques.

Enabling diffraction propagation in Chatoyant requires additional parameters in the message class. The class now contains the user's requested optical propagation method (ray, Gauss, or scalar diffractive), along with the complex wavefront of the beam as it propagates through the system. The wavefront is gridded, defining the degree of accuracy of the model of the wave. As with the Gaussian propagation, it is the component's responsibility to alter the wavefront as the component interacts with the light beam and return the result back into the message class.

We have currently implemented the Rayleigh-Sommerfeld diffractive formulation, using a 96-point Gaussian quadrature method for our integration technique. In Fig. 9, we show simulation results of a 850 *nm* plane wave propagating though a 50 μm aperture and striking an observation plane 300 μm away. We compare our simulations with a 80×80 "base case" from MathCAD, which uses a Romberg integration technique. The table in Fig. 9 shows the computation time and relative error of the system (compared with the base case) for different grid spacing. Using our integration technique we can decrease the computation time an order of magnitude and still remain within 2% accuracy.

3. Simulations and Analyses Of Optical MEM Systems

In this section, we show how Chatoyant can model and simulate complete mixed-signal systems. The first system uses both electrical and optical signals to simulate a complete 4*f* optoelectronic link. The second example, building from the two signal 4*f* link, adds mechanical signals for simulation and analysis of an optical MEM system. This set of example systems is centered on an optical MEM scanning mirror. With this device we are able to simulate an optical scanning system and a self-aligning optical detection system. These systems show Chatoyant's ability to model a mixed system of mechanical MEMs, optics, and electronic feedback.

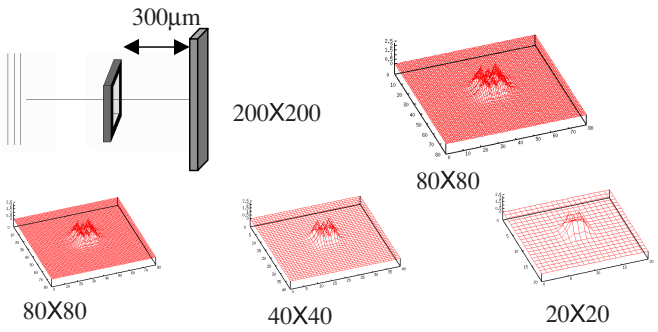

	Chatoyant		MathCAD	
	Time(*min*)	**Error(%)***	**Time(*min*)**	**Error(%)***
160x160	17.75	X	X	X
80x80	4.45	0.637	120	0
40x40	.1	1.67	20	1.54
20x20	0.29	3.37	7	4.32

*RMS Error of grid cells with respect to 80x80 MathCAD

Fig. 9: Computation Time vs. Accuracy using Chatoyant's Scalar Propagation Models.

3.1. Full Link Example

A complete optoelectronic simulation of a 4*f* optical communication link in Chatoyant is presented in Fig. 10. The distance between the VSCEL array and the first lens, and the distance between the second lens and the detector array are both 1 *mm*. The distance between the lenses is 2 *mm*, with both lenses having a focal length of 1 *mm*. The top third of the figure shows the system as represented in Chatoyant. Each icon represents a component model, and each line represents a signal path (either optical or electrical) connecting the outputs of one component to the inputs of the next. Several of the icons, such as the VCSELs and receivers, model the optoelectronic components themselves, while others, such as the output graph, are used to monitor and display the behavior of the system. The input to the system is an electrical signal with speed varying from 300 *MHz* to 1.5 *GHz*. A Gaussian noise with variance of 0.5 *V* has been added to the multistage driver system to show the ability of our models to respond to arbitrary waveforms.

In the center of the figure, three snapshots (before the VCSEL, after the VCSEL, and after the detector) show the behavior of the CMOS drivers under a 300 *MHz* noisy signal. In these snapshots, one can see the amplification of the system noise through the CMOS drivers, the clipping of sub-threshold noise in the VCSEL, and the frequency response on the quality of the received signal. This last observation is better seen in the three eye diagrams, shown in the bottom of Fig. 10, analyzed at 300 *MHz*, 900 *MHz*, and 1.5 *GHz*. For the component values chosen, the system operates with reasonable BER up to about 1 *GHz*.

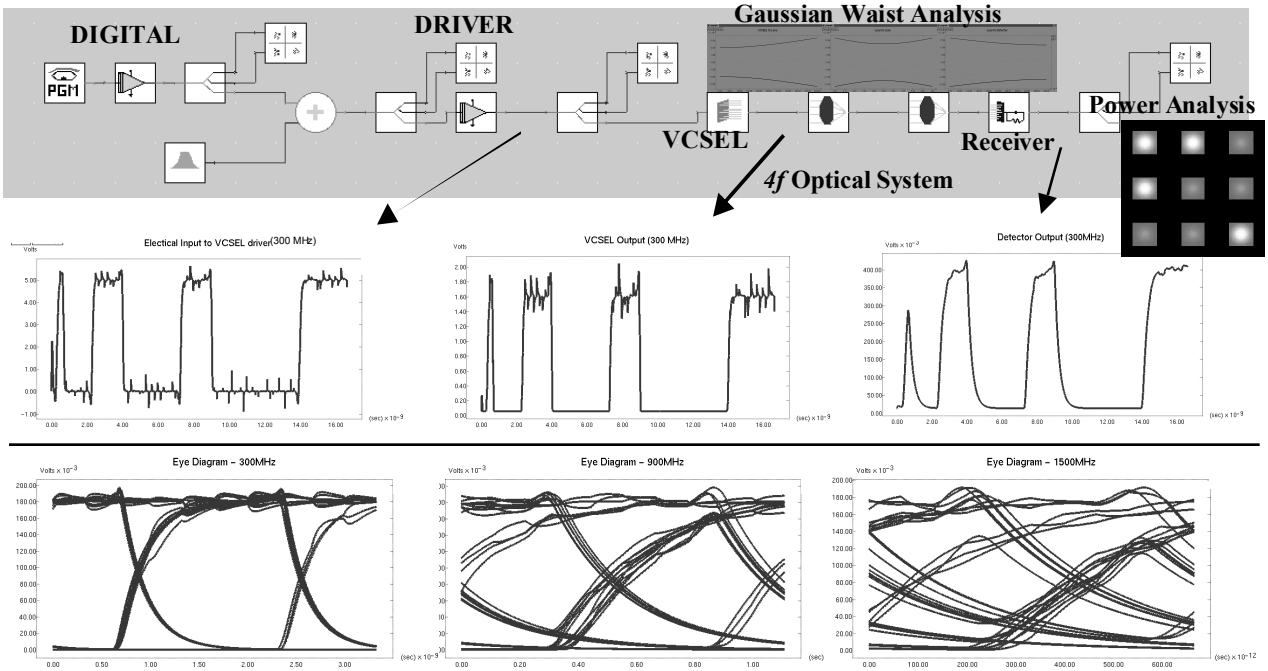

Fig. 10: Chatoyant Analysis of an Opto-electronic 4*f* Communications Link.

For this 4*f* system, the VCSEL and driver circuits explicitly model the effects of bias current and temperature on the L-I efficiency of the lasers. Fig. 11 shows the effects of temperature, T, and current bias, I_b, on the BER of the link. Generally, the frequency response of the link is dominated by the design of the receiver circuit, however it is interesting to note that both the VCSEL temperature and bias have a significant effect on system performance, due to their impact in the power through the link. Perhaps most interesting is the fact that increasing bias current does not always correspond to better performance over the whole range of frequencies examined. Note that the curve for 1 *mA* bias offers the best performance below 600 *MHz*, however the 0.5 *mA* bias (the nominal threshold of the VCSEL), crosses the curve for 1 *mA* and achieves the best performance at higher frequencies.

As an example of our mechanical tolerancing, we analyze the system with varying sized photo-detectors (50, 30, and 20 μm). The detectors are displaced from ±10 μm to ±100 μm in detector position along the axis of optical propagation. This results in defocusing of the beam relative to the detector array. We calculate both the insertion loss and the worst case optical crosstalk as the detectors are displaced. The results are shown in Fig. 12. System components can be analyzed for their sensitivity to mechanical tolerances using our Monte Carlo tolerancing method described in [3,4].

Two additional optical analyses are also shown in the Chatoyant representation in Fig. 10. The first is the beam profile analysis, which graphically displays one beam's waist as it propagates between components, showing the possibility of clipping at the lenses. The second analysis shows the optical signals as they strike the detector array. This analysis also gives the user the amount of optical power captured on each of the detectors. From this analysis, optical crosstalk and system insertion loss can be calculated.

3.2. Optical Beam Steering/Alignment System

An optical MEM component that we have modeled in Chatoyant and used in system level simulations is a torsion-scanning mirror. This is a micromachined 2D mirror built upon a Micro Elevator by Self Assembly (MESA) structure [31,32]. The mirror and MESA structure are shown in Fig. 13 (a) and (b), respectively. The scanning mirror can tilt along the torsion bars in both the x and y directions and is controlled electrostatically through four electrodes beneath the mirror, outlined in Fig. 13 (a) by the dashed boxes. For example, the mirror tilts in the positive x direction when voltage is applied to electrodes 1 and 2, and the mirror tilts in the negative y direction when voltage is applied to electrodes 1 and 4. The MESA structure is shown in Fig. 13 (b). The mirror is elevated by four scratch drive accuators (SDA) [33] sets pushing the support plates together, allowing for the scanning mirror to buckle and rise up off the substrate. The MESA structure's height is required to be large enough such that the tilt of the mirror will not cause the mirror to hit the substrate. System alignment can also be possibly aided by this MESA structure.

Fig. 14 shows the torsion-scanning mirror system that we are simulating with Chatoyant. VCSELs emit light vertically through a prism and reflects off a plane mirror. The light is then reflected off of the optical MEM scanning mirror, back to the plane mirror, and captured through a prism onto detectors. With the flexibility of the scanning mirror, this system could act as a switch, an optical scanner, or a reconfigurable optical interconnect. We have simulated systems using this scanning mirror configuration for switching and self-alignment through optical feedback. We first demonstrate an optical scanning system.

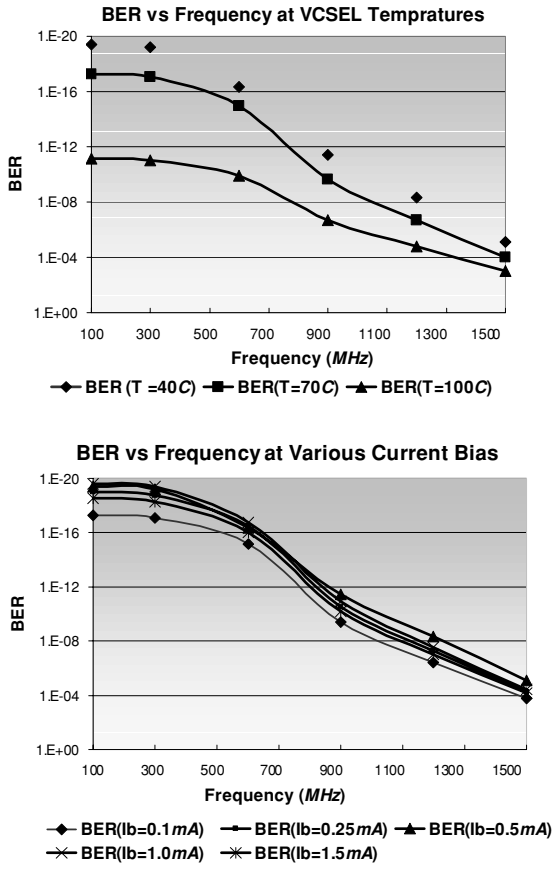

Fig. 11: BER vs. Frequency at Different VCSEL Temperatures and Current Biases.

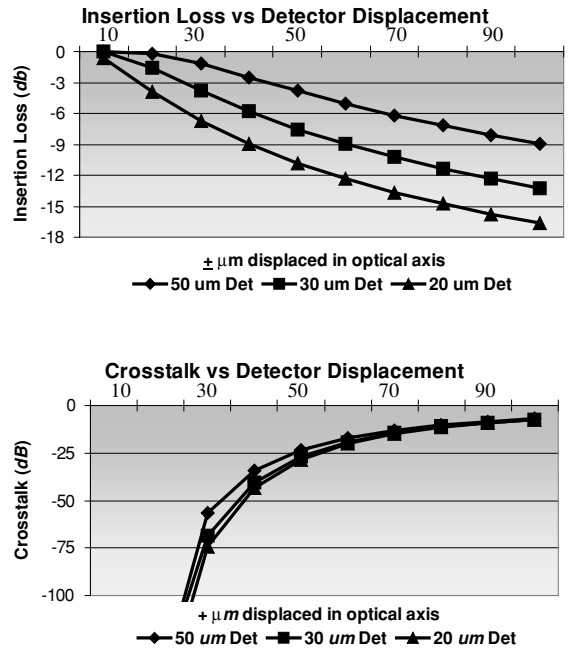

Fig. 12: Insertion and Crosstalk vs. Mechanical Tolerancing.

In this scanning system, we simulate a single source beam propagating through a 3×3 sub-system of Fig. 14. With the appropriate voltage levels applied to the four electrodes, the scanning mirror tilts and directs the source to any of the nine detectors. This system, as represented in Chatoyant, is shown in Fig. 15. The SDA arrays move the mirror to the correct height for alignment. We control the electrodes with a waveform generator, which applies the appropriate voltages on the four electrodes for the beam to scan or switch in a desired pattern. As an example, we are able to scan a diamond pattern with the waveforms shown in Fig. 16. The desired pattern is shown by the white arrow trace on the first output image. The other nine images show snapshots of the detector plane as the diamond pattern is scanned. Dashed lettered lines correspond time intervals in the waveforms and in the snapshots. Mechanical alignment is critical in this system. For example, the lenslets in this simulation are only 100 μm in diameter. Therefore, when steering the beam, precision in the voltage waveforms is needed so that the light, bending through the prism, hits the desired detector's lenslet.

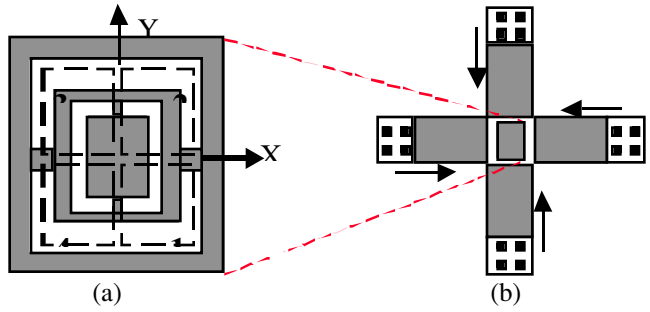

Fig. 13: Scanning Torsion Mirror and MESA Structure.

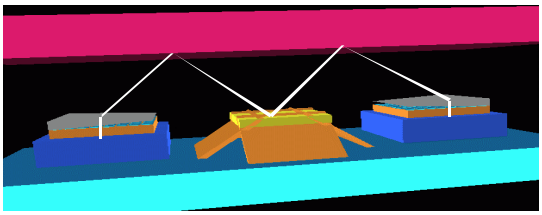

Fig. 14: Scanning Mirror System.

We next simulate a self-aligning system using optical feedback, using the same system set-up as seen in Fig. 14. Such a system could be used as a noise suppression system. The scanning mirror is used to actively align the system, with the electrodes now being controlled by a waveform generator with a programmed control algorithm. The waveform generator receives the power values detected on each of the detectors, determines where the beam is, and which electrodes to apply voltage to in order to steer the beam onto the center detector. The system is considered aligned when the power detected on the center detector matches a threshold value set by the user. The user also specifies in the control algorithm, the size of the voltage step that will be placed on the corresponding electrodes. With active feedback, the system will keep stepping enough voltage to the electrodes until the beam is steered onto the center detector and the system is aligned. The system, as displayed in Chatoyant, is shown in Fig. 17.

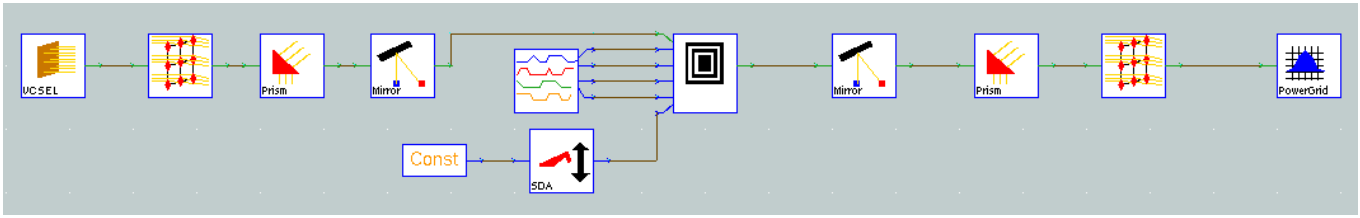

Fig. 15: Scanning System Represented in Chatoyant.

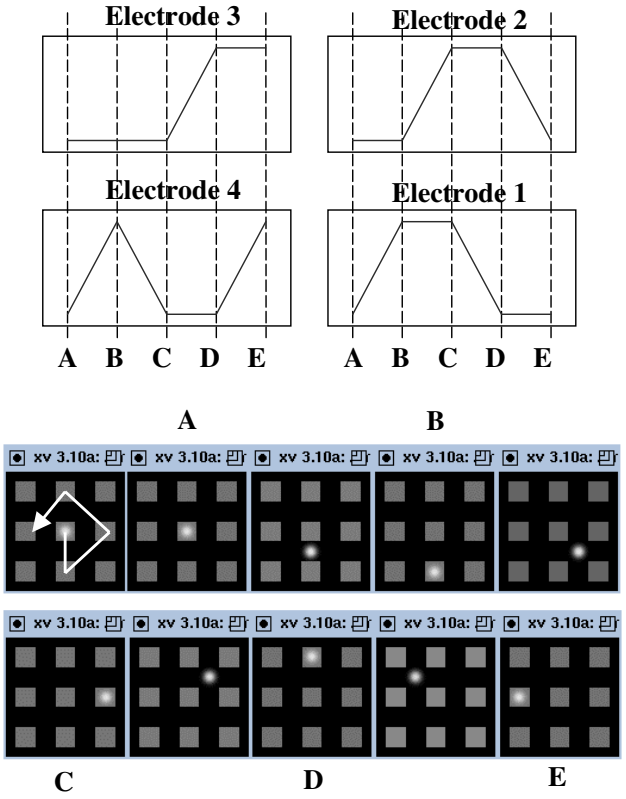

Fig. 16: Scanning Waveforms and Scanned Diamond Pattern.

To simulate this self-aligning system, we introduced random offsets in the lenses and in the VCSEL position and observe as the beam moves towards focus on the center detector. Snapshots of the image at the detectors are given in Figure 18 for three cases. The first results, shown in Figure 18(a), is when the second lens is offset 35 μm in the x direction. Figure 18(b) shows the results of the second lenslet offset in both the $-x$ and y direction by 35 μm. The final case has both lenses offset. The first is offset by 5 μm in the x direction, and the second lens is offset by 35 μm in the $-x$ direction and 5 μm in the y direction. The results are seen in Figure 18(c). Notice that the beam on the final images is not exactly in the center of the middle detector. This is due to the power being detected at this point exceeding the power threshold (98.6%) we set for alignment.

4. Summary and Conclusions

Multi-domain modeling and multi-rate simulation tools are required to support mixed technology system design. This paper has shown Chatoyant's support for simulating and analyzing optical MEM systems with models for optical, electrical, and mechanical models for components and signals. By supporting a variety of component and signal modeling techniques and multiple abstraction levels, Chatoyant has the ability to perform and analyze mixed-signal trade-offs, which makes it valuable to optical MEM designers. Keeping simulations, along with analysis techniques such as Monte Carlo for mechanical tolerancing, BER, crosstalk, and insertion loss, within the Chatoyant framework allows for quick and efficient analysis throughout multiple domains.

Acknowledgments

This work was supported by DARPA, under Grant No. F3602-97-2-0122 and NSF, under Grant No. ECS-9616879.

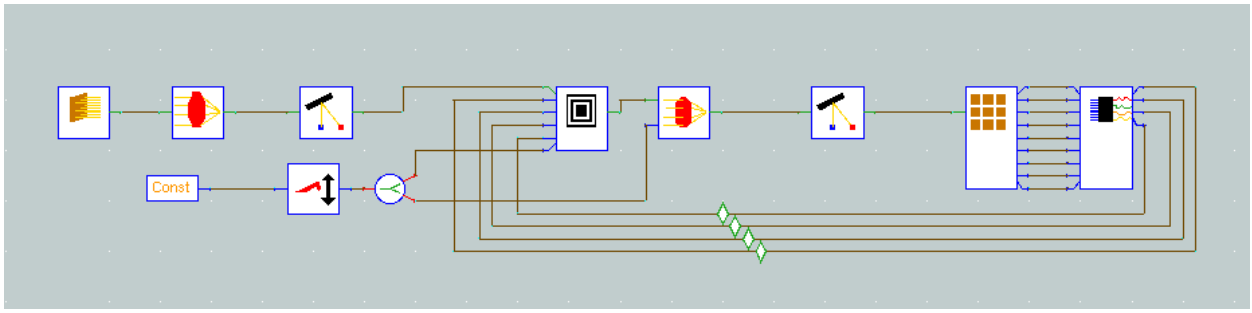

Fig. 17: Self-aligning System Using Optical Feedback.

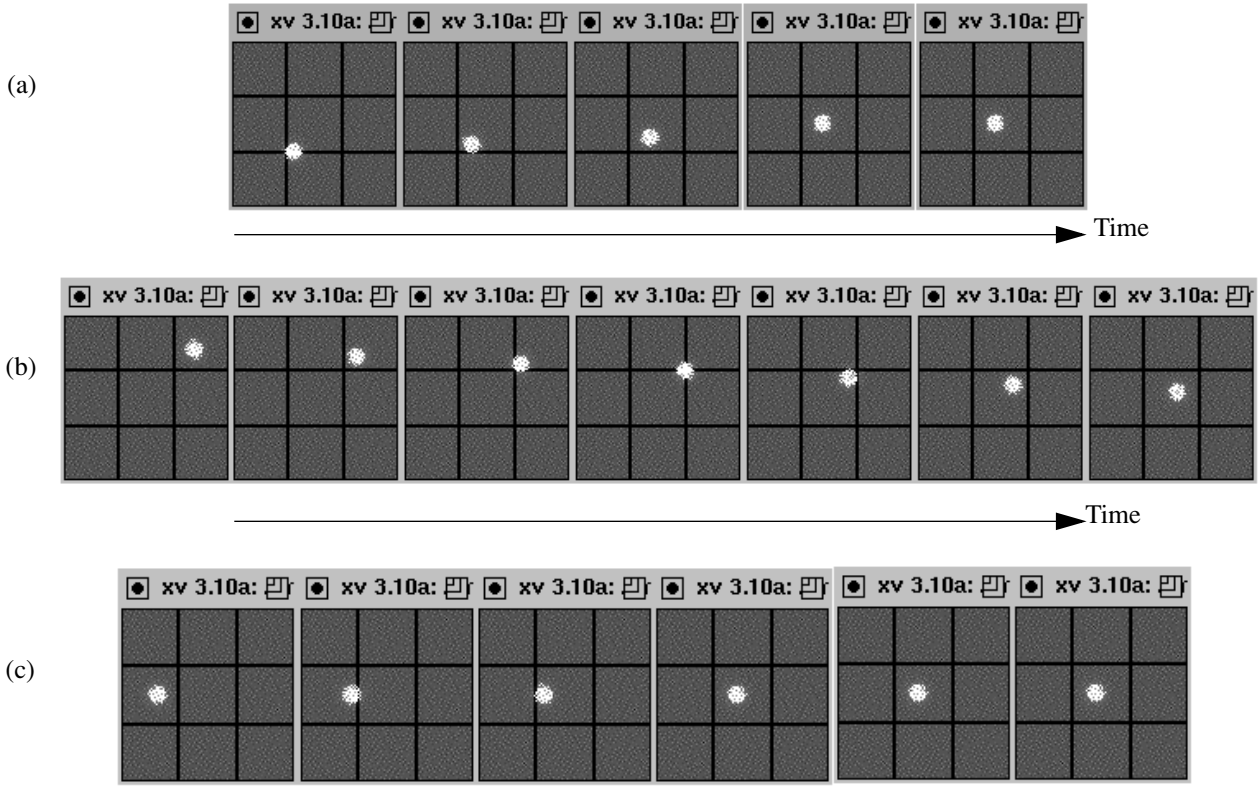

Fig. 18: Self alignment Results.

References

[1] S. P. Levitan, T. P. Kurzweg, P. J. Marchand, M. A. Rempel, D. M. Chiarulli, J. A. Martinez, J. M. Bridgen, C. Fan, F. B. McCormick, "Chatoyant: a computer-aided design tool for free-space optoelectronic systems," Applied Optics, Vol. 37, No. 26, September, 1998, pp. 6078-6092.

[2] S. P. Levitan, P. J. Marchand, T. P. Kurzweg, M. A. Rempel, D. M. Chiarulli, C. Fan, F. B. McCormick, "Computer-Aided Design of Free-Space Opto-Electronic Systems," Proceedings of the 1997 Design Automation Conference, Anaheim, CA, June 1997, Best Paper Award, pp. 768-773.

[3] T. P. Kurzweg, S. P. Levitan, P. J. Marchand, J. A. Martinez, K. R. Prough, D. M. Chiarulli, "CAD for Optical MEMS," Proceedings of the 36th IEEE/ACM Design Automation Conference (DAC'99), New Orleans, LA, June 20-25, 1999.

[4] T. P. Kurzweg, S. P. Levitan, P. J. Marchand, J. A. Martinez, K. R. Prough, D. M. Chiarulli., "Modeling and Simulating Optical MEMS using Chatoyant," Design, Test, and Microfabrication of MEMS/MOEMS, Paris, France, March 30 - April 1, 1999.

[5] J. A. Martinez, S. P. Levitan, T. P. Kurzweg, E. N. Reiss, M. T. Shomsky, P. J. Marchand, D. M. Chiarulli, "Modeling Free Space Optoelectronic Interconnects," IEEE Conference on Parallel Interconnects (PI'99), Anchorage, Alaska, October 17-19, 1999.

[6] J. Buck, S. Ha, E. A. Lee, Messerschmitt, D., "Ptolemy: a framework for simulating and prototyping heterogeneous systems," Int. J. Computer Simulation, Vol. 4, 1994, pp. 155-182.

[7] J. Morikuni, S. Kang, Computer -Aided Design of Optoelectronic Integrated Circuits and Systems, Prentice-Hall, Inc., New Jersey, Chapter 6, 1997.

[8] E. M. Buturla, P. E. Cottrell, B. M. Grossman, K. A. Salsburg, "Finite element analysis of semiconductor devices: the FIELDAY program," IBM Journal of Research and Development, vol. 25, 1981, pp. 218-231.

[9] M. R. Pinto, C. S. Rafferty, R. W. Dutton, "PISCES II - Poisson and continuity equation solver," Stanford Electronics Laboratory Technical Report, Standard University, September 1984.

[10] P. C. H Chan and C. T. Sah, "Exact equivalent circuit model for steady-state characterization of semiconductor devices with multiple energy-level recombination centers," IEEE Transactions of Electronic Devices, Vol. ED-26, 1979, pp. 924-936.

[11] R. Kielkowski, "SPICE, Overcoming the obstacles of circuit simulation," McGraw-Hill, Inc., chapter 4. 1994.

[12] S. Kim, N. Gopal, L. T. Pillage, "Time-Domain Macromodels for VLSI Interconnect Analysis," IEEE Tran.

on CAD of Integrated Circuits and Systems, Vol. 13, No. 10, pp. 1257-1270, October 1994.

[13] A. Devgan and R. A. Rohrer, "Adaptively Controlled Explicit Simulation," IEEE Tran. on CAD of Integrated Circuits and Systems, pp. 746-762, June 1994.

[14] P. Feldmann and R. W. Freund, "Efficient linear circuit analysis by PadÈ approximation via the Lanczos process," IEEE Trans. Computer-Aided Design, vol. 14, pp. 639-649, May. 1995.

[15] A. Odabasioglu, M. Celik, L. T. Pileggi, "PRIMA: Passive Reduced-Order Interconnect Macromodeling Algorithm," IEEE Trans. Computer-Aided Design, vol. 17, No. 8, 1998, pp 645-654.

[16] L. T. Pillage and R. A. Rohrer, "Asymptotic waveform evaluation for timing analysis," IEEE Trans. Computer-Aided Design, vol. 9, No. 4, pp. 352-366, Apr. 1990.

[17] L. W. Nagel,"SPICE2, a computer program to simulate semiconductor circuits," Tech. Rep. Memo UCB/ ERL M520, Univ. of California, Berkeley, CA, May 1975.

[18] A. Salz and M. Horowitz, "IRSIM: an Incremental MOS Switch-Level Simulator," Proceedings of the 26th Design Automation Conference, pp. 173-178, 1989.

[19] R. Kao and M. Horowitz, "Timing Analysis for Piecewise Linear Rsim," IEEE Trans. Computer-Aided Design, vol. 13, No. 12, 1994, pp 1498-1512.

[20] J. Vlach and K. Singhai, Computer Methods for Circuit Analysis and Design.

[21] J. Clark, N. Zhou, S. Brown, and K. S. J. Pister, "Nodal Analysis for MEMS Simulation and Design," Proc. Modeling and Simulation of Microsystems Workshop, Santa Clara, CA, April 6-8, 1998.

[22] J. E. Vandemeer, "Nodal Design of Actuators and Sensors (NODAS)", M.S. Thesis, (Department of Electrical and Computer Engineering, Carniege Mellon University, Pittsburgh, PA., 1997).

[23] J. E. Vandemeer, M. S. Kranz, G. K. Fedder, "Hierarchical Representation and Simulation of Micromachined Inertial Sensors," Proc. Modeling and Simulation of Microsystems Workshop, Santa Clara, CA, April 6-8, 1998.

[24] W. J. Duncan, "Reciprocation of Triply Partitioned Matricies," J. Roy. Aeron. Soc., vol. 60, 1956, pp. 131-132.

[25] J. S. Przemieniecki, Theory of Matrix Structural Analysis, (McGraw-Hill, New York, New York, 1968).

[26] B. E. A Saleh and M. C. Teich, Fundamentals of Photonics (New York: Wiley-Interscience, 1991).

[27] S. J. Walker and D. J. Nagel, "Optics & MEMS," Navel Research Lab, NRL/MR/6336-99-7975

[28] M. Born, E. Wolf, Principles of Optics, (Pergamon Press, 1959).

[29] J. W. Goodman, Introduction to Fourier Optics, Second Edition (The McGraw-Hill Companies, Inc., 1996).

[30] E. Hecht, Optics, Second Edition (Addison-Wesley Publishing Company, 1987).

[31] M. C. Wu, "Micromachining for optical and Optoelectronic Systems," Proceedings of the IEEE, Vol. 85, No. 11, (November 1997), pp. 1833-1856.

[32] W. Piyawattanametha, L. Fan, S. S. Lee, J. G. D. Su, M. C. Wu, "MEMS Technology for Optical Crosslink for Micro/Nano Satellites," International Conference of Integrated Nano/Microtechnolgy for Space Applications (NANOSPACE98), NASA/Johnson Space Center, Houston, TX, Nov 1-6, 1998.

[33] T. Akiyama, D. Collard, H. Fujita, "Scratch drive actuator with mechanical links for self-assembly of three-dimensional MEMS," Journal of Microelectromechanical Systems, Vol. 6, No. 1., March 1997, pp. 10-17.

Received in Cambridge, MA, USA, November 13 1999

Paper 2/01775